The Superior Olivary Nucleus and Its Influence on Nucleus Laminaris: A Source of Inhibitory Feedback for Coincidence Detection in the Avian Auditory Brainstem

Lichuan Yang, Pablo Monsivais, and Edwin W Rubel

Virginia Merrill Bloedel Hearing Research Center and Department of Otolaryngology-Head and Neck Surgery, University of Washington, Seattle, Washington 98195

Located in the ventrolateral region of the avian brainstem, the superior olivary nucleus (SON) receives inputs from nucleus angularis (NA) and nucleus laminaris (NL) and projects back to NA, NL, and nucleus magnocellularis (NM). The reciprocal connections between the SON and NL are of particular interest because they constitute a feedback circuit for coincidence detection. In the present study, the chick SON was investigated. *In vivo* tracing studies show that the SON projects predominantly to the ipsilateral NM, NL, and NA. *In vitro* whole-cell recording reveals single-cell morphology, firing properties, and postsynaptic responses. SON neurons are morphologically and physiologically suited for temporal integration; their firing patterns do not reflect the temporal structure of their excitatory inputs. Of most interest, direct stimulation of the SON evokes long-lasting inhibition in NL neurons. The inhibition blocks both intrinsic spike generation and orthodromically evoked activity in NL neurons and can be eliminated by bicuculline methiodide, a potent antagonist for GABA_A receptor-mediated neurotransmission. These results strongly suggest that the SON provides GABAergic inhibitory feedback to laminaris neurons. We discuss a mechanism whereby SON-evoked GABAergic inhibition can influence the coding of interaural time differences for sound localization in the avian auditory brainstem.

Key words: avian superior olivary nucleus; GABAergic inhibition; coincidence detection; nucleus laminaris; membrane conductance; shunting effect

In the avian auditory brainstem there are four primary nuclei for acoustic processing. Nucleus magnocellularis (NM) and nucleus angularis (NA) receive direct excitatory inputs from the auditory nerve (Boord, 1969; Ramón y Cajal, 1971; Rubel and Parks, 1975; Parks and Rubel, 1978; Jhaveri and Morest, 1982a,b; Carr and Boudreau, 1991). NM neurons send bilateral excitatory projections to nucleus laminaris (NL), a group of cells specialized for coincidence detection of interaural delays (Boord, 1969; Parks and Rubel, 1975; Smith and Rubel, 1979; Young and Rubel, 1983; Carr and Konishi, 1988, 1990; Overholt et al., 1992; Joseph and Hyson, 1993). NA neurons do not innervate NL but send direct ascending projections to the lateral lemniscal complex and inferior colliculus (Conlee and Parks, 1986; Takahashi and Konishi, 1988). Located in the ventrolateral brainstem and slightly rostral to the level of NL is the superior olivary nucleus (SON). It receives inputs from NA and NL and projects back to NM, NA, and NL (Takahashi and Konishi, 1988; Carr et al., 1989; Carr and Boudreau, 1993; Lachica et al., 1994).

Previous studies of the avian auditory brainstem have emphasized the morphological and physiological specialization of NM and NL neurons for binaural processing (Parks and Rubel, 1975; Rubel and Parks, 1975; Smith and Rubel, 1979; Hackett et al., 1982; Jackson and Parks, 1982; Young and Rubel, 1983; Sullivan and Konishi, 1984; Carr and Konishi, 1990; Warchol and Dallos,

1990; Raman and Trussell, 1992; Trussell et al., 1993; Raman et al., 1994; Reyes et al., 1994, 1996). These studies have yielded a substantial quantity of data showing that both NM and NL neurons are suited for the task of coincidence detection. In addition, several lines of evidence have suggested that GABAergic inhibition is involved in the process. For instance, intercalated among the connections between NM and NL is a dense network of terminals containing the inhibitory neurotransmitter GABA (Müller, 1987; Carr et al., 1989; Code et al., 1989; von Bartheld et al., 1989; Hyson and Sadler, 1995). In chicks at embryonic day 15 (E15) and older, GABAergic terminals are abundant among NM and NL neurons. They surround neuronal somata and make synaptic contacts (Parks, 1981; Code et al., 1989, 1991; Lachica et al., 1994). The sources of these GABAergic terminals have been identified. A number of stellate cells surrounding NM and NL are stained positively for GABA and provide some of the GABAergic terminals on magnocellularis and laminaris neurons (von Bartheld et al., 1989; Carr et al., 1989). However, the majority of GABAergic terminals in NM, NL, and NA originate from the SON. Lachica et al. (1994) have shown that most SON neurons in chicks are positively stained for GABA. SON neurons project to NM, NL, and NA and terminate in patterns that resemble the distribution of GABA-immunoreactive puncta seen in these three nuclei. Because the SON receives inputs from NA and NL, the reciprocal connections between the SON and NL imply that the SON provides a feedback regulation and directly affects the coding of interaural time differences by NL neurons (Lachica et al., 1994; Peña et al., 1996). Several physiological studies have shown that NL and NM neurons do receive GABAergic influence (Fujita and Konishi, 1991; Hyson et al., 1995; Lu et al., 1997; Funabiki et al., 1998). Bath application of GABA or stimulating GABAergic terminals near NM and NL causes NM and NL

neurons to depolarize. The depolarization is apparently mediated by efflux of Cl^- ions and is blockable by bicuculline, an antagonist for $GABA_A$ receptors (Lu et al., 1997; Funabiki et al., 1998). Those studies did not identify the source of the observed GABAergic inhibition, although it was presumed to be from the SON. The present study is an initial step toward understanding the function of the SON in the avian auditory brainstem.

MATERIALS AND METHODS

Experiments were performed using both *in vivo* (10- to 12-d-old postnatal chicken) and *in vitro* preparations (E18- to E20-d-old). *In vivo* studies were aimed at further characterizing the projection pattern of the SON into NA, NM, and NL. *In vitro* studies investigated the physiology and morphology of single SON cells. Both techniques have been described previously (Hyson and Rubel, 1989; Overholt et al., 1992; Lachica et al., 1994; Reyes et al., 1994, 1996). Methods are briefly described below.

Surgical procedures and tracer injection. Four white leghorn hatching chickens (*Gallus gallus*) at 10- to 12-d-old were anesthetized by intraperitoneal injection of ketamine (8 mg/100 gm) and Nembutal (1.8 mg/100 gm). Supplemental anesthesia was administrated at half the original dose every 60 min. The feathers on the head were trimmed short and then removed with a depilatory. The head was secured in a head holder attached to a stereotaxic apparatus. The skin and muscles overlying the skull were reflected, and Lidocaine (Elkins-Sinn) was applied topically to all open wounds. The surface of the skull was cleared of tissue, and a large craniotomy was performed to expose the dorsal surface of the cerebellum. After ligating the central sinus, the dura was reflected. Subsequently, the whole cerebellum was removed by aspiration. With the cerebellum removed, the dorsal surface of brainstem was visible with clear landmarks for the location of the incoming auditory nerve, NM and NL. A glass pipette with a tip diameter of $20–40$ μm was filled with 10% lysine-fixable dextran conjugated to fluorescein (3 kDa, pH 7.4; Molecular Probes, Eugene, OR) or tetramethylrhodamine (3 kDa, pH 7.4; Molecular Probes). The pipette was visually guided to the area of NM and NL. Multiple pressure injections of tracer were made with a total volume of $0.2–0.3$ μl. In each animal, one color of tracer was injected on one side, and the other color of tracer was immediately injected on the other side at the corresponding location in the brainstem. After survival times of 18 (one case), 24 (two cases), and 42 (one case) hr, the animals were deeply anesthetized with a lethal dose of Nembutal. Animals were then perfused transcardially with PBS (0.1 M, pH 7.4) followed by a fixative solution of 4% paraformaldehyde. After fixation, the brain was dissected out, post-fixed for 2 hr, and then transferred to a 30% sucrose solution overnight for cryoprotection. The brain was sectioned on a freezing microtome at a thickness of 40 μm. Sections were then mounted on slides and coverslipped with Dako glycergel mounting medium.

Sections were evaluated with epi-illumination using appropriate filter cubes. The fluorescence of cells filled with dextran conjugated to tetramethylrhodamine (red) were typically more intense than cells filled with dextran conjugated to fluorescein (green). Moreover, the wavelengths passed by the fluorescein cube could also evoke a slight fluorescence in the cells strongly stained by rhodamine. To ensure that double-labeled cells could be distinguished from such bleed-over, in two additional animals we injected both rhodamine- and fluorescein-conjugated dextran in the same side of the brainstem. The labeled SON cells in these two cases fluoresced intensely when viewed with both cubes. This served as a standard, and we considered cells as double-labeled only when clear fluorescence was observed with both cubes.

Brain slice preparation. Chickens of ages E18–E20 were rapidly decapitated. A 4 mm segment of the skull containing the brainstem was removed with a razor blade and quickly submerged in ice-cold artificial CSF (ACSF). ACSF contained (in mM): 130 NaCl, 26 NaH_2CO_3, 3 KCl, 2 $CaCl_2$, 1 $MgCl_2$, 1.25 NaH_2PO_4, and 10 dextrose. The brainstem segment was dissected out and transferred to a Vibratome tissue slicer (Pelco, St. Louis, MO) where it was mounted on an agar block with cyanoacrylate glue and cut in ice-cold ACSF. Five 200 μm coronal slices containing the SON, NL, and NM were collected and incubated in a holding chamber filled with ACSF at room temperature (22–23°C). ACSF was constantly gassed with 95% O_2 and 5% CO_2 and had a pH of 7.4.

Whole-cell recording. Slices were transferred to a 0.5 cc recording chamber mounted on a Zeiss Axioskop FS with a 40× water-immersion objective and infrared, DIC optics (Zeiss, Germany) and superfused

with ACSF at a rate of 3 ml/min. Using a multiple valve system, a slice was perfused with normal ACSF or ACSF containing 50 μM bicuculline methiodide (Sigma, St. Louis, MO).

All recordings were performed at room temperature (22–23°C). Patch pipettes were drawn from 75 μl hematocrit tubing (VWR Scientific, San Francisco, CA) using a two-stage electrode puller. The pipette tips were heat polished and had resistances between 4 and 8 $M\Omega$ (DC). Pipettes were filled with intracellular pipette solution that contained (in mM): 105 K-gluconate, 35 KCl, 5 EGTA, 10 K-HEPES, and 1 $MgCl_2$. The pH of the solution was adjusted to 7.2 with KOH. Biocytin (Sigma) was then added to the solution (final concentration was 0.145%), and osmolality was measured between 280 and 290 mOsm. The junction potential for this intracellular pipette solution was 7 mV with reference to the grounded bath medium. All data are presented with correction for the junction potential.

Whole-cell voltage signals were recorded under current clamp using an Axoclamp 2B microelectrode amplifier (Axon Instruments, Burlingame, CA). Tight seals (>1 $G\Omega$) were established on the somata of visually identified neurons by applying slight negative pressure to the recording pipette after contact with the cell surface. The formation of $G\Omega$ seals and the subsequent rupturing of the underlying membrane were monitored in voltage-clamp mode by measuring the resistive current resulting from a high-frequency, -5 mV pulse command. Stable recordings could be maintained up to 2 hr. During recordings, we periodically monitored series resistance and capacitive currents to ensure good electrical access to the interior of the cell. Recordings were aborted if the membrane potential of a neuron depolarized to -40 mV or greater, and/or if a ruptured patch "resealed" and could not be ruptured again.

Data were low-pass filtered at 10 kHz and digitized with an ITC-16 (Instrutech, Great Neck, NY) at 20 kHz for both on- and off-line analysis. All recording protocols were written and run using the acquisition and analysis software Synapse, version 2.2 (Synergy, Bethesda, MD). Analyses were subsequently performed in Synapse and Cricket Graph (Cricket Software, Malvern, PA).

Extracellular stimulation. Concentric bipolar electrodes (Frederick Haer) with tip diameter of 0.5 mm were used for extracellular stimulation. In one experimental configuration, the electrode was placed at the fiber tract from NL and NA to the SON at a distance of 0.5–1 mm away from the SON to study the postsynaptic responses of SON cells. In another experimental configuration, the stimulating electrode was placed directly on the SON to study the effect of the SON activation on NL neurons (see Fig. 2*B*). Square electric pulses of 100 μsec duration were delivered through a stimulus isolation unit and interval generator (WPI 1830). The intensity was varied from 10–90 V at 10 V increments.

Single-cell labeling. After whole-cell recording, biocytin was injected into individual SON neurons through the recording pipette. Biocytin diffused into the cell during recording, but we enhanced the loading by passing positive current pulses of $+0.2$ to $+0.6$ nA repetitively for 10 min. Afterward, slices were continuously incubated in oxygenated ACSF at room temperature for up to 2 hr. Slices were then fixed in 4% paraformaldehyde. After rinsing in PBS, the slices were treated with 1% H_2O_2 for 30 min to eliminate endogenous peroxidase. The slices were rinsed again and then immersed in 0.3% Triton X-100 for 1 hr. After removing Triton X-100, the slices were treated by the ABC procedure (Vectastain ABC Elite kit; Vector Laboratories, Burlingame, CA) followed by DAB reaction. Slices were then mounted, air-dried, and dehydrated through an ascending ethanol series, cleared in xylene, and coverslipped using Permount. Biocytin-labeled SON cells were examined under bright-field light microscopy.

Table 1. Retrogradely labeled SON neurons

	Ipsilateral SON	Contralateral SON
Fluorescein-labeled	372	22
Rhodamine-labeled	743	29
Double-labeled	0	0
Total labeled cells	111 (96%)	51 (4%)

Number of labeled SON cells in four animals after one tracer was injected on one side of the brainstem, and the other tracer was injected into the same area on the other side of the brainstem.
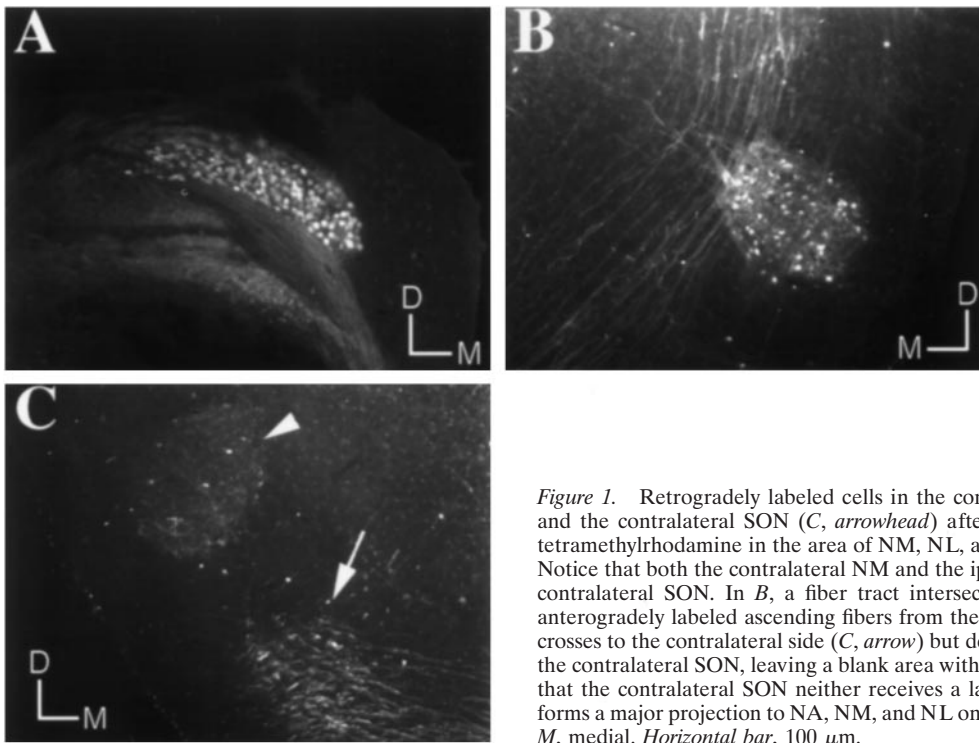
Figure 1. Retrogradely labeled cells in the contralateral NM (*A*), the ipsilateral SON (*B*), and the contralateral SON (*C*, *arrowhead*) after a large injection of dextran conjugated to tetramethylrhodamine in the area of NM, NL, and a portion of NA on one side of brainstem. Notice that both the contralateral NM and the ipsilateral SON are heavily labeled but not the contralateral SON. In *B*, a fiber tract intersects with the ipsilateral SON, which contains anterogradely labeled ascending fibers from the ipsilateral NL and NA. The same fiber tract crosses to the contralateral side (*C*, *arrow*) but detours and projects anteriorly before reaching the contralateral SON, leaving a blank area with few visibly labeled fibers. These images show that the contralateral SON neither receives a large number of inputs from NA and NL nor forms a major projection to NA, NM, and NL on the opposite side of the brainstem. *D*, Dorsal; *M*, medial. *Horizontal bar*, 100 μm.
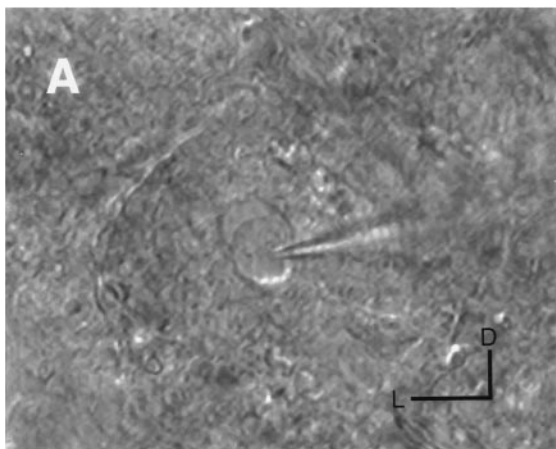
Table 2. Electrical characteristics of SON neurons

Resting potential (mV)	-59.6 ± 5.7
R_n (MΩ)[a]	234 ± 49.6
t (msec)[b]	26.7 ± 15.7
Spike threshold (mV)	-43.7 ± 6.3
Spike amplitude (mV)	56.1 ± 11.7

Characteristics of SON neurons ($n = 23$) recorded whole-cell in brainstem slices. Mean $\pm$ SD. Input resistance was calculated from the slope of *I–V* function in response to hyperpolarizing current injection. The response to -0.1 nA current injection was fit to double exponential curve, and the time constant was calculated based on the faster exponential. Spike threshold was measured as the voltage at which the rapid upstroke of the action potential began. Spike amplitude was calculated as the peak voltage of the action potential minus the spike threshold.

[a]R_n = input resistance.

[b]t = time constant.

←
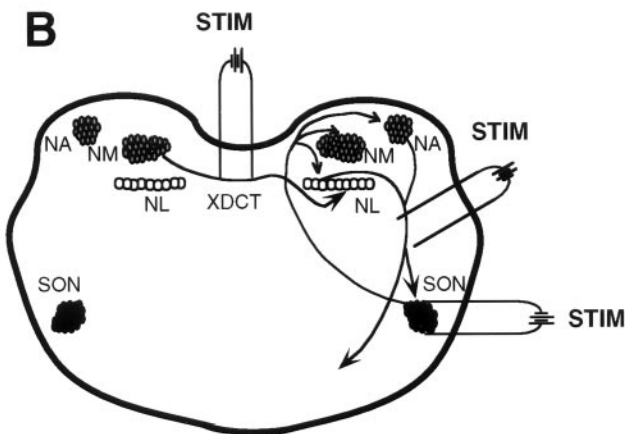
Figure 2. *A*, Infrared DIC image of an individual SON neuron under whole-cell recording configuration. *B*, Circuit showing the connections between the SON and three dorsal auditory nuclei. Based on previous and present studies, the SON receives ipsilateral inputs from the ascending fiber tract of NA and NL and projects back to NL, NM, and NA on the same side (*arrow lines*). NL receives bilateral inputs from NM. The contralateral NM innervates NL neurons through the crossed dorsal cochlear tract (*XDCT*). *STIM*, The position of stimulating electrodes in the three experimental situations described in the Materials and Methods. *D*, Dorsal; *L*, lateral. *Horizontal bar*, 20 μm.
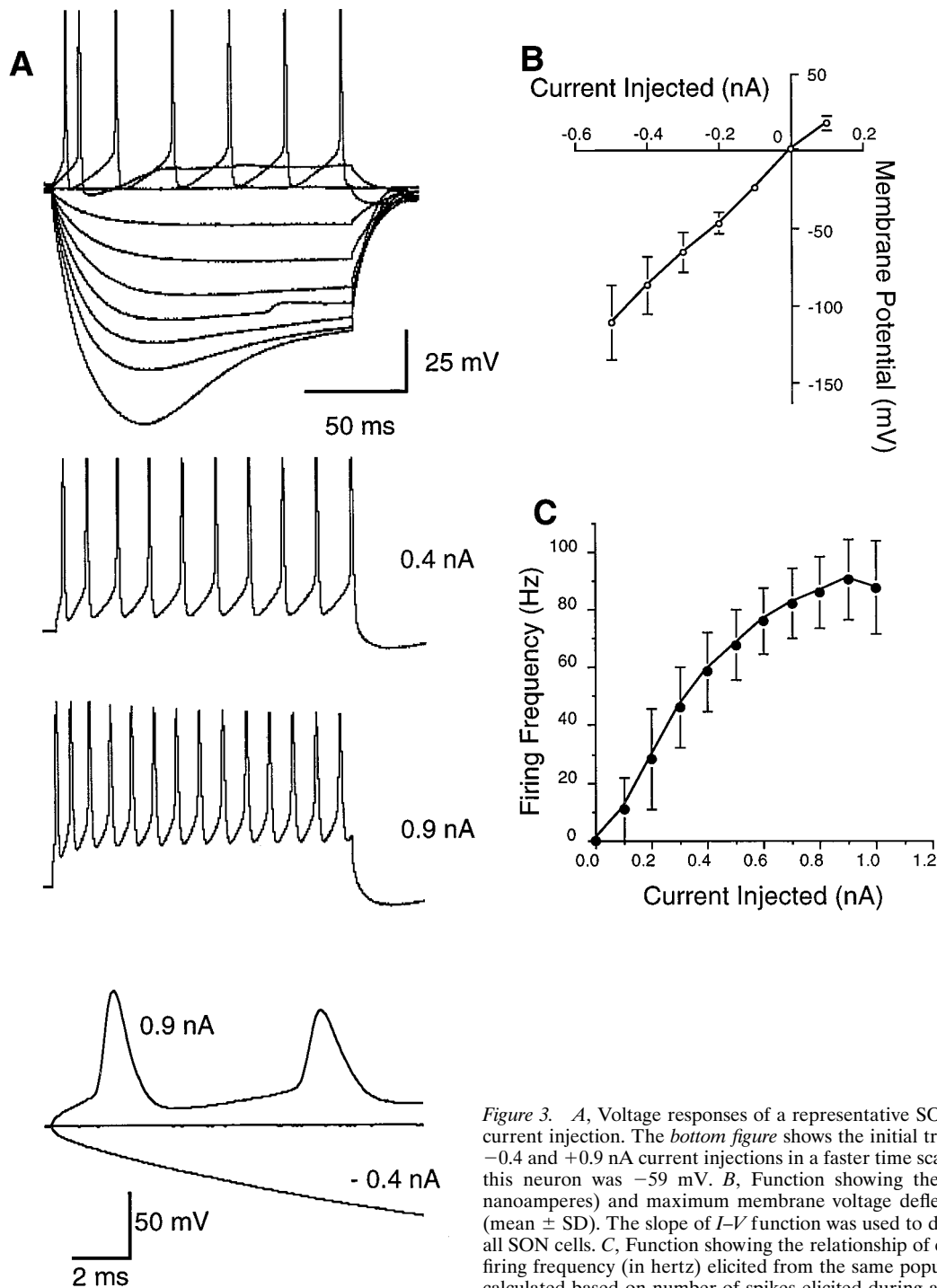
Figure 3. *A*, Voltage responses of a representative SON neuron to 150 msec steps of steady current injection. The *bottom figure* shows the initial traces of the responses of the neuron to −0.4 and +0.9 nA current injections in a faster time scale. The resting membrane potential of this neuron was −59 mV. *B*, Function showing the relationship of current injected (in nanoamperes) and maximum membrane voltage deflection (in millivolts) for 23 SON cells (mean ± SD). The slope of *I–V* function was used to determine the mean input resistance of all SON cells. *C*, Function showing the relationship of current injected (in nanoamperes) and firing frequency (in hertz) elicited from the same population of neurons. Firing frequency is calculated based on number of spikes elicited during a 150 msec current injection period.

RESULTS

Four types of experiments were conducted to address the following issues. (1) *In vivo* injection of dextran conjugated to fluorescein in the area of NM and NL on one side of the brainstem and dextran conjugated to tetramethylrhodamine in the same area on the other side of the brainstem. We intended to confirm the results of a previous study (Lachica et al., 1994) showing that SON neurons project bilaterally to NM, NA, and NL. In addition, we wanted to know if single SON neurons project bilaterally or unilaterally by looking for double-labeled cells in the SON. (2) *In vitro* whole-cell current-clamp record-

ings were obtained from SON neurons. We studied the firing properties of SON neurons in response to current injection and subsequently labeled the cells with biocytin to identify their morphology and axonal trajectory. (3) We electrically stimulated the fiber bundle that contains axons from NL and NA innervating the SON to characterize the postsynaptic responses of SON neurons. (4) We evaluated the influence of SON input on NL neurons in two ways; first by stimulating SON directly while activating NL neurons by current injection; and second by simultaneously stimulating SON and the excitatory (NM) input to NL while recording from NL neurons.
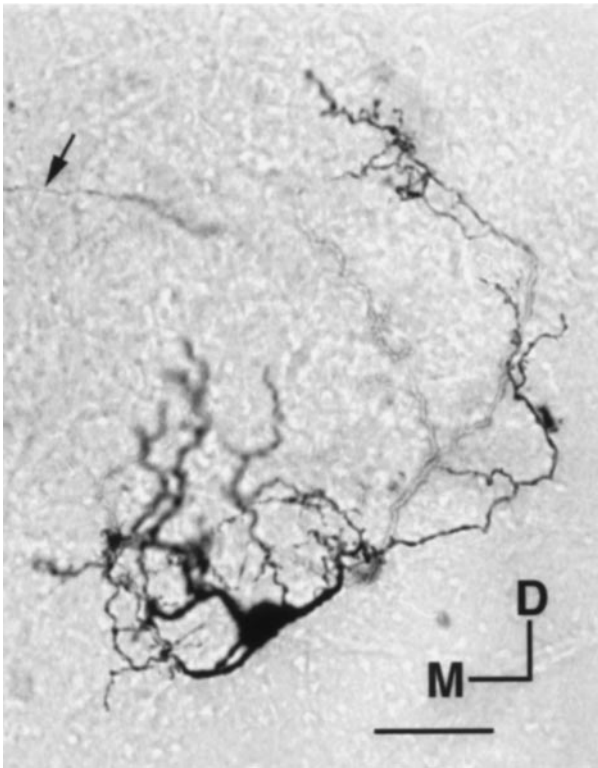
Figure 4. Photomicrograph of an SON neuron labeled with biocytin. The *arrow* points to the projecting axon. Scale bar, 30 μm. *M*, Medial; *D*, dorsal.

SON neurons project predominantly to the ipsilateral NM, NL, and NA

Previous studies of the SON projections in the auditory brainstem are contradictory. In barn owl, Carr et al. (1989) and Takahashi and Konishi (1988) have shown that SON neurons project mainly

to the ipsilateral NM, NA, and NL. Lachica et al. (1994), however, have shown that SON neurons in chicks not only project ipsilaterally to NL, NM, and NA but also to the same targets at the contralateral side. To clarify this issue, we did double-labeling experiments.

Table 1 summarizes the result from four animals in which dextran conjugated to fluorescein (green) was injected on one side of the brainstem, and dextran conjugated to tetramethylrhodamine (red) was injected into the same area on the other side of the brainstem. The injection sites were relatively large and included NM and NL as well as a portion of NA and some parts of the medial and ventral vestibular nuclei. In four animals receiving such double injections, 1166 SON cells were labeled by either fluorescein or rhodamine. We never observed double-labeled cells. Surprisingly, the majority (96%) of labeled cells were found in the SON ipsilateral to the injection site of a given color. Only a small percent (4%) of the labeled cells were located in the contralateral SON. These results strongly suggest that SON neurons project predominantly to the ipsilateral NM, NL, and NA areas. Furthermore, the lack of double labeling in the SON indicates that the contralateral projection must derive from a very small number of SON cells and that these cells do not project to the ipsilateral side as well.

The predominance of ipsilateral labeling is further illustrated in Figure 1. Figure 1*A* shows NM contralateral to a rhodamine injection site. The intensive labeling of almost all NM cells suggests that the injection site was large enough to cover the entire region of NL that was innervated by the contralateral NM and forms a convenient positive control. Figure 1, *B* and *C*, shows the ipsilateral and contralateral SON, respectively, from the same animal. Although a large number of cells were labeled in the ipsilateral SON, very few cells were labeled in the contralateral SON. As evident in Figure 1*B*, the ipsilateral SON intersects with a ventrally projecting fiber tract. This fiber tract contains anterogradely labeled ascending fibers from NL and NA neurons. The innervation of SON neurons presumably comes from collaterals
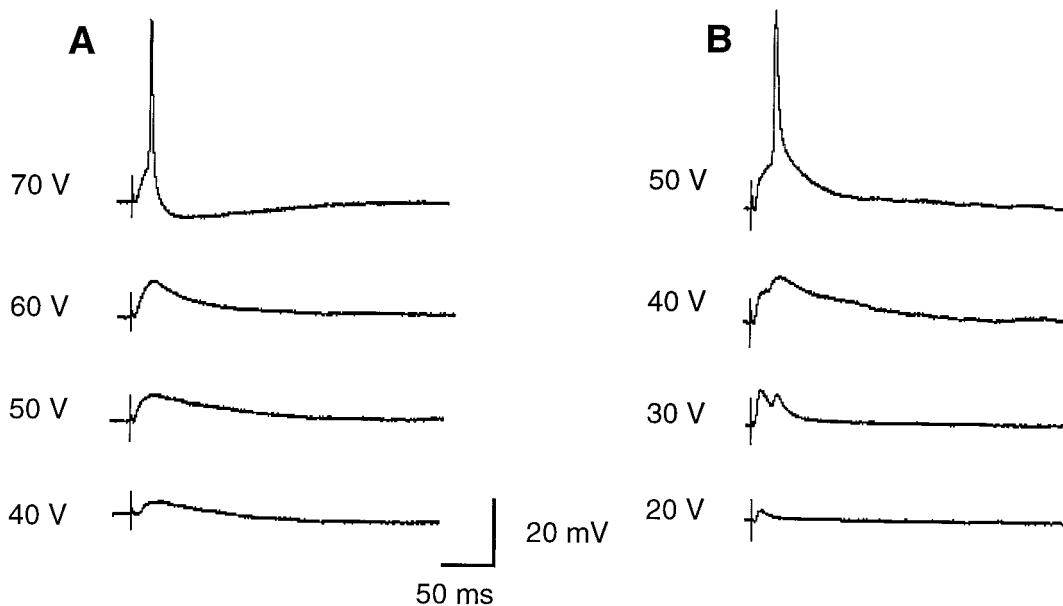
Figure 5. EPSPs evoked at different stimulus intensities for two representative SON neurons. The neuron in *A* shows graded EPSPs with smooth rise and fall. The neuron in *B* exhibits summation of multiple unitary EPSPs, especially at stimulus intensities of 30 and 40 V. The stimulus artifacts were truncated for clarity. The resting membrane potential was −56 mV for the neuron in *A* and −60 mV for the neuron in *B*.

Single Stimulus

70 V

60 V

20 mV

50 ms

Repetitive Stimuli (Hz)

25 Hz

50 Hz

100 Hz

200 Hz
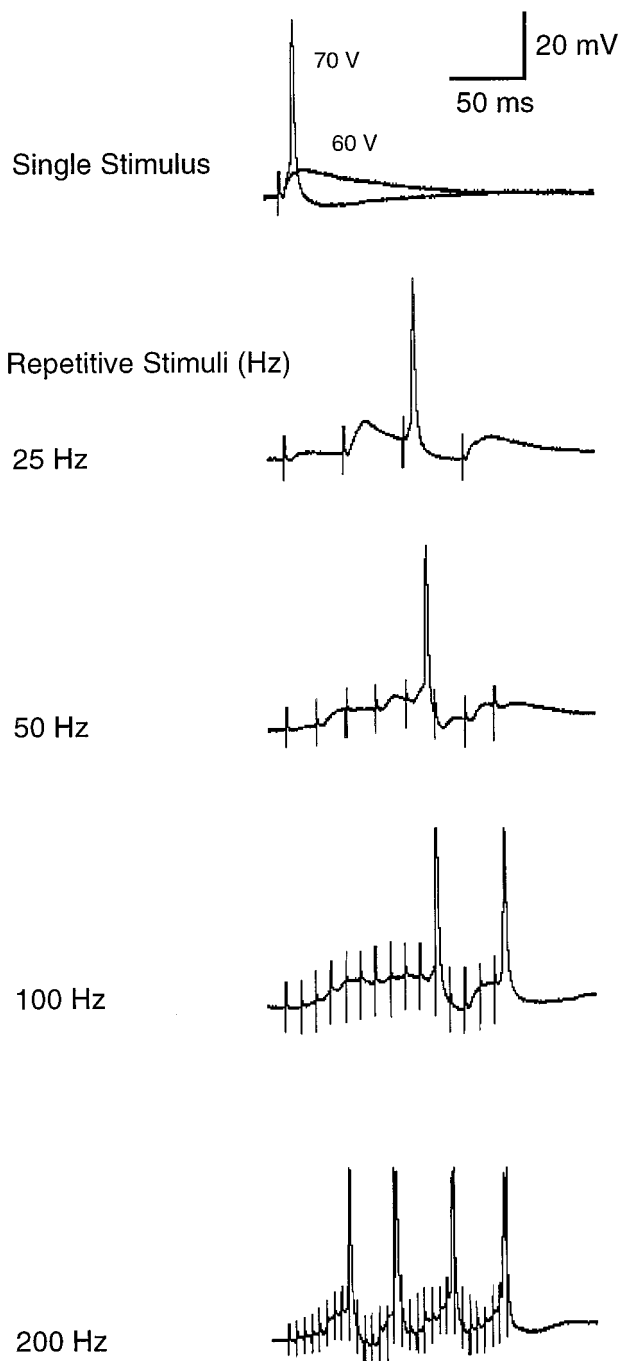
Figure 6. Temporal summation of EPSPs in an SON neuron in response to repetitive subthreshold stimulation. *Top trace* shows the response of the neuron to single pulse stimulation at 60 and 70 V. Stimulus intensity was then held at 60 V (subthreshold) and applied repetitively at different frequencies. The stimulus artifacts were truncated for clarity. Notice that temporal summation occurred even at 25 Hz and gave rise to an action potential. Temporal summation became more prominent at higher frequencies, causing the cell to discharge more action potentials during the stimulus train. The resting membrane potential was −54 mV.

of the main tract, which continues ventrally and eventually crosses the midline to the contralateral side (Fig. 1*C*). The same fiber tract detours and projects anteriorly before reaching the contralateral SON, leaving a blank area with few visible axons. This pattern of labeling suggests that the contralateral SON at this level neither receives a large number of inputs from nor projects strongly to the SON, NA, NM, or NL on the opposite side.

Firing properties and morphology of single SON neurons

Single SON cells were studied in a brain slice preparation (Fig. 2*A*). After whole-cell configuration was established, we first studied the firing properties of each cell in response to steps of negative and positive current injection. Subsequently, biocytin was injected into the cell, and its morphology was later characterized. We recorded a total of 60 SON cells. Of this population, 23 cells fulfilled our criteria and were used for analysis. The characteristics of these cells are listed in Table 2.

SON neurons showed a high degree of homogeneity with respect to their firing properties and morphology. As shown by data from a representative SON neuron in Figure 3*A*, large negative current injection (more than −0.6 nA) caused a "sag" in its hyperpolarizing membrane potential. That is, the steady-state voltage deflection was less than the initial transient deflection. The "sag" was not evoked at lower hyperpolarizing currents, leaving only the steady-state voltage deflection. Measurement made at the peaks of each voltage curve showed an approximately linear *I–V* function that gave a membrane resistance of 188 MΩ for this neuron to the hyperpolarizing current injection. Injection of positive current as low as 0.1 nA caused the neuron to fire a single action potential (Fig. 3*A*). With further increases in the current strength, the cell fired for the duration of the current step, and firing rate was proportional to the current magnitude; the number of action potentials increased, and interspike interval decreased (Fig. 3*A*). At large positive current levels (more than +0.8 nA), the firing rate saturated, and the amplitudes of the later spikes became smaller than those of the initial spikes. Nevertheless, there appeared to be little spike-frequency adaptation (Fig. 3*A*). Figure 3, *B* and *C*, shows, respectively, the membrane voltage deflection as a function of current injected (*B*) and the firing frequency as a function of current injected (*C*) for 23 SON neurons (Mean ± SD). All SON neurons had relatively high input resistance and fired at a rate proportional to current strength.

Biocytin-labeled SON cells (20) were multipolar with at least three dendrites that ramified extensively inside the nucleus. Frequently, an axon could be identified first traveling medially across the space of the ascending fiber tract of NL and NA (Fig. 1*B*) and then projecting dorsally. The projecting axons were strictly confined to the ipsilateral side and rarely ramified along their path. We were normally able to trace the individual axons for at least 2 mm before losing them as they approached their targets, which most likely were NM, NL, and NA. Figure 4 shows a photomicrograph of a representative SON cell labeled with biocytin.

Postsynaptic responses

We studied 14 SON neurons while electrically stimulating the fiber tract that contains the ascending fibers from NL and NA (Figs. 1*B*, 2*B*). The stimulating electrode was positioned at a distance of 0.5–1 mm from the SON. Without exception, a sufficiently intense electric pulse, 100 μsec in duration, produced a depolarizing postsynaptic potential (PSP) that was proportional to the stimulus intensity. Figure 5 illustrates the effect of increasing stimulus intensity on PSPs in two SON neurons. In the first neuron, an increase in the stimulus intensity resulted in a steady increase in the magnitude of the PSP until an action potential was elicited. As was typical of all SON neurons, the action potential was preceded by a graded depolarization (Fig. 5*A*). In the second
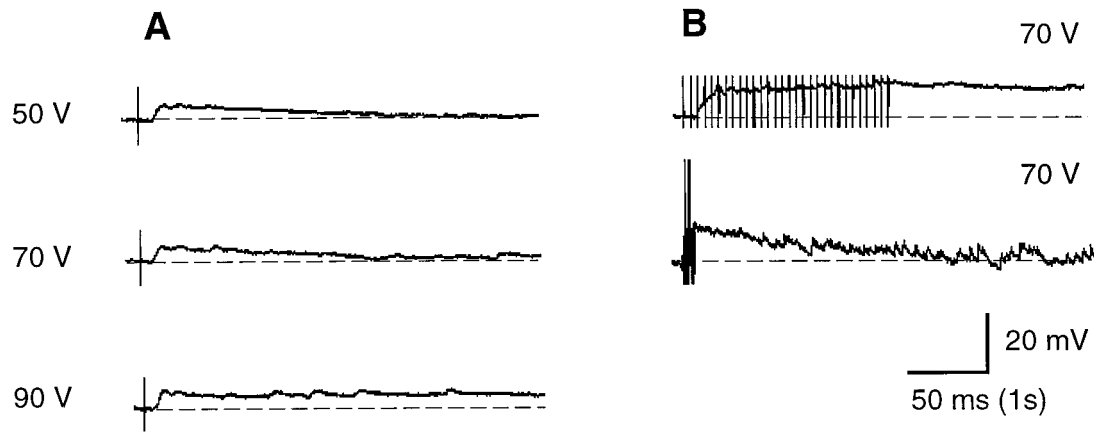
Figure 7. Recordings obtained from an NL neuron when the ipsilateral SON was electrically stimulated. *Traces* in *A* resulted from single pulse stimulation of the SON, whereas traces in *B* resulted from a 150 msec train of pulse stimuli applied to the SON at frequency of 200 Hz. The *bottom trace* in *B* shows the result using a slow acquisition time (calibration: 1 sec) for the full-scale display of SON-evoked depolarization in the recorded NL neuron. Notice the increased membrane potential fluctuation, which is probably caused by increased frequency of spontaneous PSPs in the NL neuron after SON stimulation. The resting membrane potential was −58 mV. The stimulus artifacts were truncated.

neuron, increase in the stimulus intensity also resulted in graded PSPs that led to an action potential at high stimulus intensity. But unlike the first neuron, the second neuron appeared to receive at least two PSPs that showed temporal summation (Fig. 5*B*). Neurons with such temporally summed PSPs accounted for 21% (3 of 14) of our sampled cells. All PSPs, with or without temporal summation, had relatively long duration. When the maximum EPSPs before spiking were analyzed, the mean (± SD) response latencies were 2.6 (± 0.8) msec, amplitudes were 10.0 (± 4.2) mV, rise times were 10.5 (± 4) msec, and 50% decay times were 38.6 (± 11.1) msec. For comparison, the average rise times and 50% decay times of EPSPs in five NM neurons recorded under the same conditions were 1.6 msec and 1.0 msec, respectively.

These long-lasting individual PSPs suggest that SON neurons temporally sum repetitive stimuli. Figure 6 shows one of 14 neurons in which we examined postsynaptic responses while a subthreshold stimulus was delivered repetitively. The *top trace* in Figure 6 shows the response of a neuron to a single pulse stimulation. Although stimulus intensity of 60 V evoked an EPSP, 70 V caused the neuron to discharge an action potential. We then fixed the stimulus intensity at 60 V (slightly subthreshold) and varied the stimulus frequency from 25 to 200 Hz. Even at 25 Hz, the PSPs evoked by each stimulus began to sum and produced an action potential. As frequency increased to 100 and 200 Hz, the summation became stronger, producing a plateau depolarization similar to that evoked by a low-level, steady positive current injection (Fig. 3*A*). As a consequence, the neuron discharged more action potentials (Fig. 6, *bottom trace*). This result suggests that SON neurons are capable of integrating synaptic inputs, but that any temporal information in the pattern of incoming action potentials is not well preserved.

SON-evoked response on NL neurons

To test whether the SON provides an influence on one of its postsynaptic targets, NL neurons were whole-cell current-clamped at resting potential. The PSPs of the NL neuron were then recorded while stimulating SON extracellularly (Fig. 2*B*). In 32% (20 of 63) of NL neurons, stimulating SON caused a long-lasting depolarization. In the remaining 43 NL neurons, stimulating SON produced no effect. This was probably because the connections between the SON and these NL neurons were not

preserved during slice preparation. Figure 7 shows the typical responses of a NL neuron to a single stimulus or a train of stimuli applied to the SON. Strikingly, a single stimulation of 50 V and 100 μsec duration evoked a PSP in the NL neuron that lasted >100 msec (Fig. 7*A*, *top trace*). As stimulus intensity increased to 70 V, the PSP duration lengthened (*middle trace*). Further increase of stimulus intensity to 90 V resulted in a plateau depolarization that lasted beyond our acquisition window of 250 msec (*bottom trace*). The long-lasting PSPs were even more prominent when a train of pulses were applied to the SON. As shown in Figure 7*B*, the PSP could last >3 sec after giving a 150 msec train of pulses with intensity of 70 V and frequency of 200 Hz. Such dependence on stimulus parameters was observed in all neurons that exhibited SON-evoked responses. They had a minimum duration of 60 msec and a maximum amplitude of 10–15 mV.

In addition to long duration, all SON-evoked responses were depolarizing and had long synaptic delays (5–12 msec). Assuming that SON-evoked responses were mediated by GABA$_A$ receptors, it was not surprising to see depolarizing responses because a high Cl$^-$ concentration was used in our patch electrodes (Cl$^-$ equilibrium potential was −34 mV under our recording conditions). However, as we will discuss later, the observed polarity may not just reflect an artificial setting for Cl$^-$ but the real polarity. Long synaptic delays do not necessarily suggest that SON-evoked responses in NL are not monosynaptic. Latency could be prolonged by some factors in our experimental conditions. One factor was that all recordings were made at room temperature, which would slow down axonal conduction and synaptic transmission, thus giving rise to longer synaptic delays. Also, we stimulated the SON directly, which was at least 2–3 mm away from our recording site in NL. Such long distance required additional axonal conduction time for SON input to reach NL neurons. Furthermore, if there were additional synapses between the SON and NL, the SON would have to be excitatory to activate neurons that then provide inhibitory inputs to NL. The assumption is contradictory to previous and present studies showing that SON neurons are mostly GABAergic.

Inhibitory effect of SON on NL neurons

SON-evoked depolarizing PSPs on NL neurons were inhibitory in nature. The inhibition was demonstrated in two separate sets of
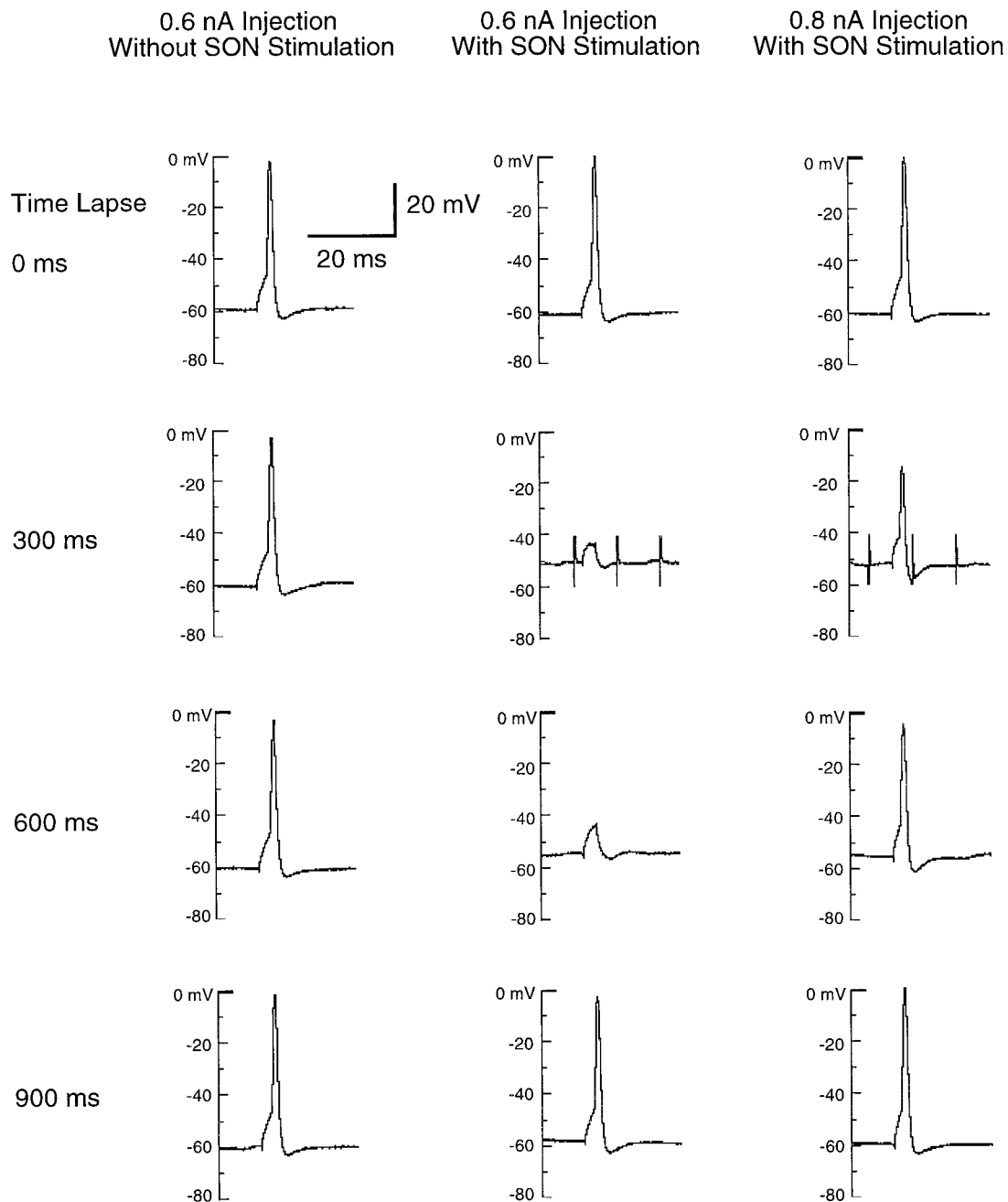
Figure 8. SON-evoked depolarization inhibits the firing of an NL neuron in response to current injection. The *left panels* show that the NL cell fired an action potential every time when a 5 msec, +0.6 nA current pulse was injected into the cell at 300 msec interval. The *middle panels* show the responses of the same cell to the same current injections during SON stimulation. SON stimulation was a 100 msec train of pulses at 60 V intensity and 100 Hz frequency, and its occurrence was marked by stimulus artifacts at the 300 msec time point (the stimulus artifacts were truncated). Notice that SON stimulation caused the membrane potential to depolarize by 10 mV from its resting potential at −60 mV and coincidentally inhibited action potential generation during SON stimulation at the 300 msec time point. The inhibition still persisted at the 600 msec time point, although SON stimulation had been terminated. By the 900 msec time point, the membrane potential had repolarized to near the resting state, and current injection was able to elicit a regular action potential. In the series shown in the *right panels*, we increased current injected to the NL cell to +0.8 nA but maintained the same regimen of SON stimulation. At the 300 and 600 msec time points, the excitation caused by current injection overcame SON-evoked inhibition so that the cell was able to fire an action potential, but the action potentials were smaller in amplitude. The blockade of action potential and reduction in spike amplitude were both attributable to the increased membrane conductance.

experiments. In one set of experiments, we injected brief current pulses into a NL neuron while providing a train of stimuli to the SON. As illustrated in Figure 8, repetitive current injections (5 msec in duration and +0.6 nA in amplitude) were used to evoke spiking in a NL neuron every 300 msec (Fig. 8, *left panel*). After

stimulating SON at the 300 msec time point (*middle panel*, marked by stimulus artifacts), the NL neuron ceased firing action potentials. The inhibition persisted at the 600 msec time point but diminished by the 900 msec time point. The blockade of action potentials was correlated with the strength of current injected and

A 0 mV

Response to -0.2nA current injection
without SON stimulation

-20

-40

-60

-80

B 0 mV

Response to -0.2nA current injection
during SON stimulation

-20

-40

-60

-80

20 mV

10 ms
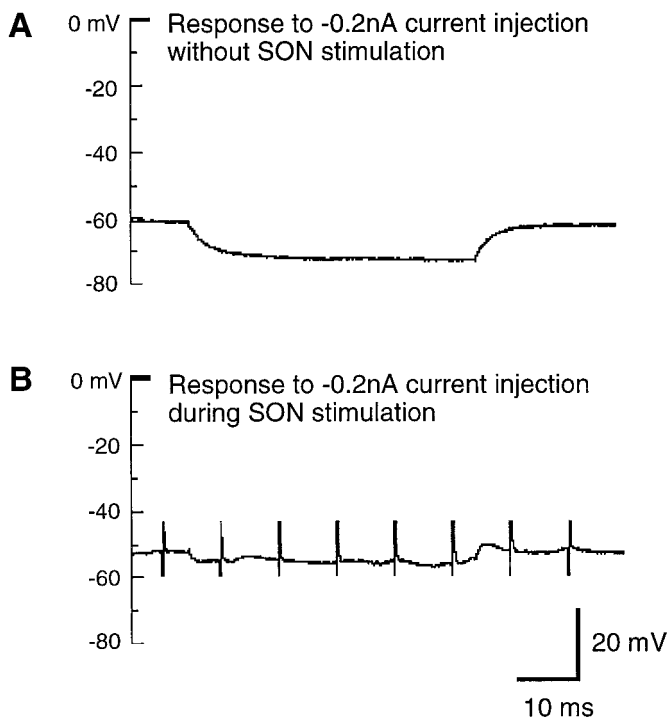
Figure 9. SON-evoked inhibition reduces the input resistance of an NL neuron. The membrane voltage deflection of the same NL neuron in Figure 8 during a 50 msec step of current injection (-0.2 nA) before (*A*) and during (*B*) SON stimulation. SON stimulation was a 100 msec train of pulses at 60 V and 100 Hz. Notice that during SON stimulation the same amount of current caused much smaller membrane voltage deflection, indicating a significant decrease of the input resistance of this neuron from 57 to 21 MΩ. The resting membrane potential was -60 mV.

also the amplitude and duration of SON-evoked depolarization. As we increased the injected current to $+0.8$ nA, the same stimulation of the SON no longer blocked the firing of the neuron (*right panel*), although the amplitude of the action potential became smaller. Most likely, SON-evoked depolarization blocked the firing of the NL neuron by decreasing membrane input resistance, therefore creating a shunting effect on the NL neuron. For this neuron, the input resistance during SON stimulation was measured by injecting a -0.2 nA current into the cell (Fig. 9). Input resistance decreased from 57 to 21 MΩ during SON stimulation. The same measurement was made in four other cells. On average, the input resistance decreased by 48% during SON stimulation, from 52 to 27 MΩ.

In the other set of experiments, instead of injecting current directly into the cell, we positioned a second stimulating electrode at the crossed dorsal cochlear tract (XDCT) that contains excitatory fibers from the contralateral NM innervating NL (Fig. 2*B*). In this way we tested directly whether SON-evoked depolarization affected the responses of NL neurons to orthodromic stimulation. As shown in Figure 10, without SON stimulation, a single stimulus at XDCT evoked an action potential at 70 V and a brief EPSP at 40 V (Fig. 10*A,C*, respectively). However, with SON stimulation, a 70 V stimulus at XDCT evoked only a small EPSP (Fig. 10*B*). In addition, with SON stimulation, the EPSP evoked by a subthreshold stimulation (40 V) became smaller in amplitude and shorter in duration (Fig. 10*D,E*). This result is consistent with what we observed in the current injection experiments described above. The SON apparently provides a strong inhibi-

tory effect on NL neurons and shapes the responses of neurons to their excitatory inputs from NM.

Pharmacology

Because most SON neurons are positively stained with a GABA antibody or an antibody against its synthetic enzyme, glutamic acid decarboxylase, SON-evoked depolarization in NL neurons observed in the present study is most likely mediated by GABAergic transmission. We bath-applied bicuculline to test whether bicuculline would eliminate SON-evoked depolarization in NL neurons. As shown in Figure 11, bicuculline at 50 μM completely blocked SON-evoked depolarization within 30 sec. The blockage was reversible within 5 min after washing. Six neurons were tested in this manner. All of them responded similarly to bicuculline application. Although not shown, bicuculline also eliminated the SON-evoked suppression of NL firing generated by direct current injection.

Bicuculline also blocked spontaneous PSPs in NL neurons. These spontaneous PSPs had a slow time course and frequently summed to produce larger depolarization lasting >200 msec (Fig. 12*A*). The slow time course of these spontaneous depolarizations suggests that they are not EPSPs generated by spontaneous release of glutamate from NM terminals but are most likely GABAergic events. The frequency of these spontaneous depolarizations increased dramatically shortly after SON stimulation, as evidenced on the *bottom trace* of Figure 7*B*. It was presumably caused by an increased spontaneous release of GABA from SON terminals or surrounding stellate GABAergic cells. Application of bicuculline eliminated these spontaneous PSPs (Fig. 12*B*).

DISCUSSION

We present four main findings. First, as in the barn owl, cells in the chick SON project predominantly to the ipsilateral NM, NL, and NA areas with only a few cells projecting to the contralateral side. Second, SON cells exhibit a high degree of morphological and functional homogeneity; all cells exhibit extensive dendritic arborization and discharge in a sustained pattern to current injection. Third, SON cells are excited by stimulation of the fiber tract containing the ascending fibers of NL and NA neurons. The postsynaptic potentials are relatively long in duration and readily sum during repetitive stimulation. Finally, direct stimulation of the SON causes a long-lasting depolarization of NL neurons. The finding that the depolarization can be blocked by bicuculline indicates that it is GABAergic. We further show that SON-evoked GABAergic inhibition exerts its influence on NL neurons through a shunting effect. These findings suggest that the SON provides an active inhibitory feedback to NL that may be important for the coding of interaural time differences. In the following sections, we will discuss the morphological and physiological features of SON cells in contrast to those of the neurons in NL and NM. We then speculate on a mechanism whereby SON-evoked inhibition can be used for the coding of interaural time differences. Finally, we will address some technical concerns and future studies that may advance our understanding of the functional properties of this circuit.

SON has different properties from NM and NL

The current study revealed three important features distinguishing SON neurons from those in NM and NL. (1) Excitatory synaptic potentials of SON neurons are slow compared with EPSPs in NM and NL and temporally sum with repetitive stimulation; (2) Unlike NM and NL neurons, which fire only single
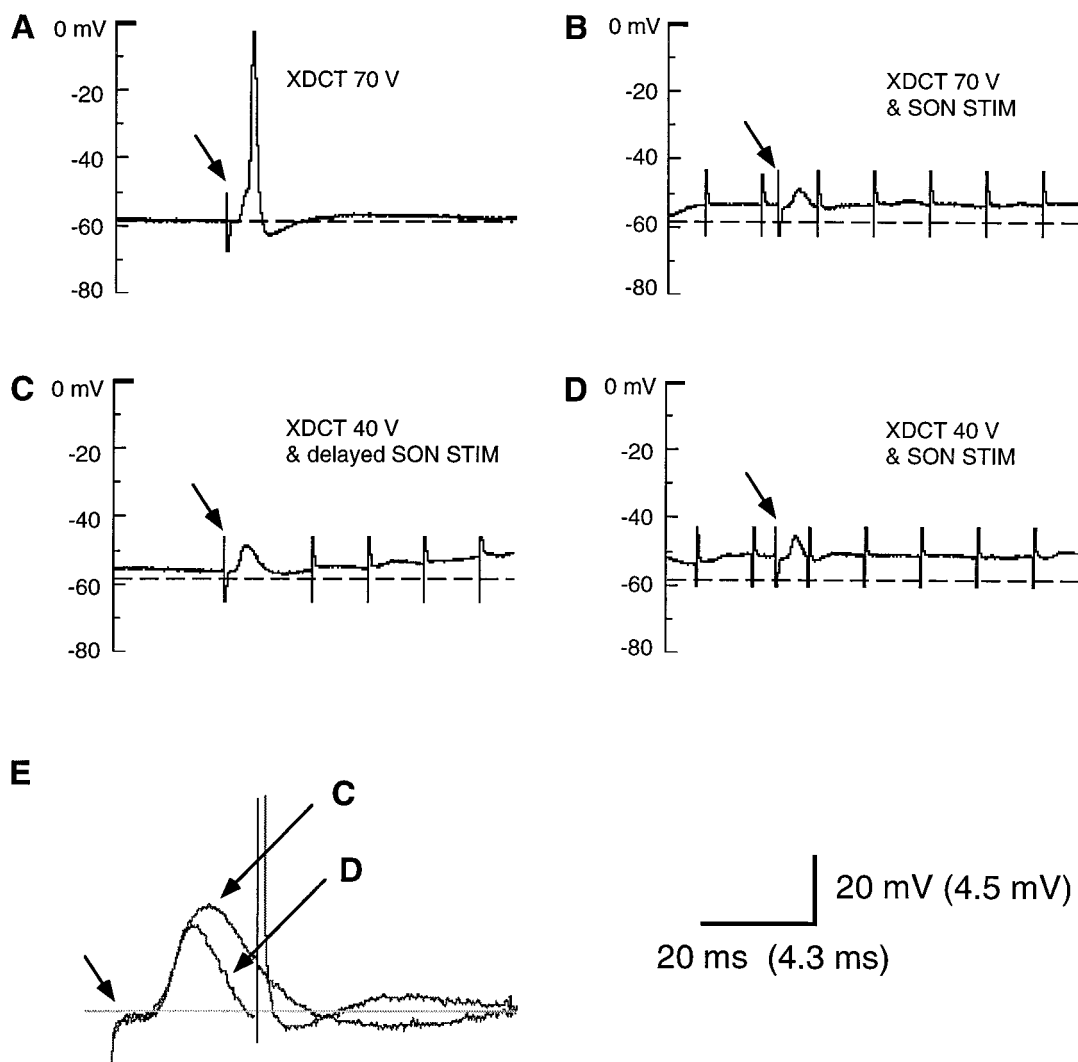
Figure 10. SON-evoked depolarization inhibits the response of an NL neuron response to its excitatory synaptic inputs. Two stimulating electrodes were used. One was positioned at the ipsilateral SON to stimulate the SON with a 100 msec train of pulses at 70 V and 100 Hz. The other electrode was positioned at the crossed dorsal cochlear tract (*XDCT*, Fig. 2*B*) to stimulate the excitatory input to the NL neuron from the contralateral NM. Whole-cell recording was performed in an NL neuron. *A* and *C* were the excitatory postsynaptic responses of the NL neuron when XDCT was stimulated with a single electric pulse at 70 and 40 V, respectively. XDCT stimulation at 70 V evoked an action potential in the NL neuron (*A*), whereas XDCT stimulation at 40 V evoked an EPSP (*C*). In *C*, SON stimulation was also applied, but delayed with respect to XDCT stimulation, therefore not affecting the EPSP generated by XDCT stimulation. *B* and *D* are the recordings with the XDCT stimulation at 70 and 40 V, respectively, and accompanied by simultaneous SON stimulation. With SON stimulation, XDCT stimulation at 70 V no longer evoked an action potential as it did in *A* but instead a small EPSP (*B*). With the same SON stimulation, the EPSP evoked by XDCT stimulation at 40 V in *C* became smaller (*D*). *E* shows the enlarged, superimposed EPSPs from *C* and *D*, notice that the amplitude and duration decreased significantly during SON stimulation. Calibration: 4.3 msec, 4.5 mV. The stimulus artifacts of XDCT stimulation are pointed by *arrows*.

spikes at the onset of current injection, SON neurons fire repetitively to depolarizing current steps at rates that are proportional to the current magnitude; (3) Morphologically, SON neurons are multipolar with expansive dendritic arborization within the nucleus, whereas neurons in NM and NL are comparatively compact. In chicks, NM neurons are largely adendritic, whereas the dendrites of NL neurons are thick, tufted, and oriented exclusively in the dorsoventral plane.

Slow postsynaptic potentials in the SON may be attributable to several factors: the location and morphology of synaptic inputs, the rate of excitatory receptor desensitization, and the time constant of the postsynaptic membrane. In chick and owl, the VIII nerve terminals form large calycine endings on somata of NM neurons (Ramón y Cajal, 1971; Parks and Rubel, 1978;

Parks, 1981; Carr and Boudreau, 1991; Köppl, 1994). Correlated with the morphology of this synapse are the findings that activation of a single VIIIth nerve fiber generates synaptic currents in NM neurons of several nanoamperes, even at depolarized holding potentials (Zhang and Trussell, 1994). The brevity of these synaptic currents is partly caused by the rapid desensitization of glutamatergic receptors on NM neurons (Raman and Trussell, 1992; Raman et al., 1994). Although our study did not examine the morphology and distribution of synapses in the SON or receptor pharmacology, the extensive dendritic arborization suggests that SON cells receive many synaptic contacts with some located distally from the soma. Thus, the rise and decay times of EPSPs in SON neurons must be influenced by the electrotonic structure of these cells (Rall, 1969). Additionally, input resistance
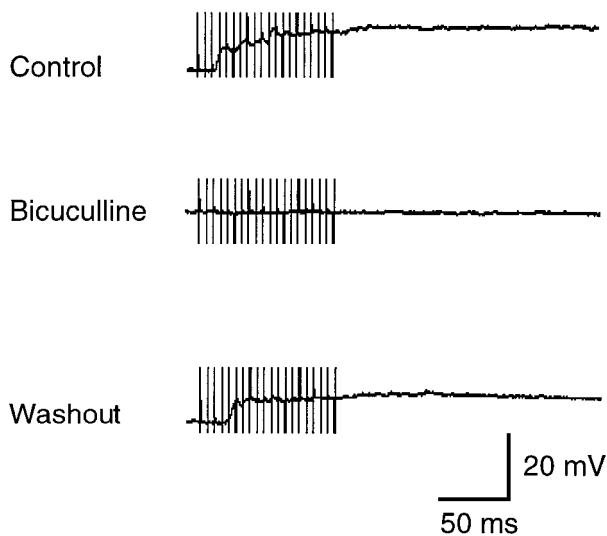
Figure 11. SON-evoked depolarization on an NL neuron before, during bicuculline application (50 μM), and after washout. The depolarization was evoked by a 100 msec train of pulses at 70 V and 200 Hz. The resting membrane potential for this neuron was -58 mV
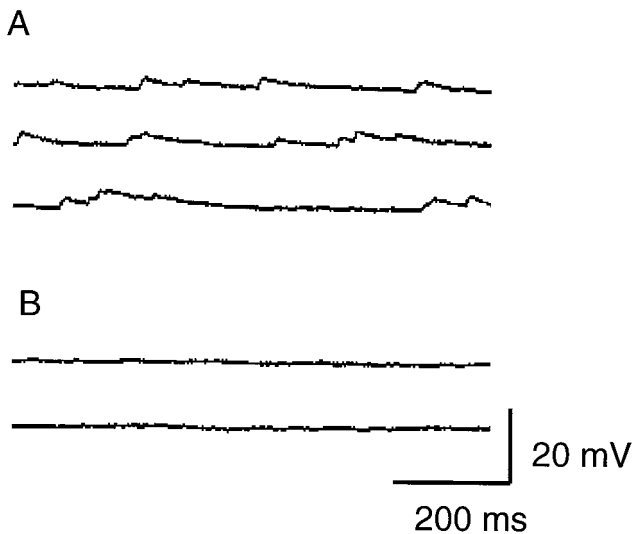
Figure 12. *A*, Spontaneous depolarizing PSPs recorded from an NL neuron without SON stimulation. Notice that the PSPs had a slow time course and frequently summed. *B*, Bicuculline (50 μM) completely eliminated these spontaneous PSPs.

of SON neurons is high compared with neurons in NM and NL, which may also contribute to the observed long time constant and slow EPSPs in SON cells.

Possible function of SON in the processing of interaural time differences

One of the most important findings of the present study is that direct stimulation of SON evoked a long-lasting, inhibitory depolarization on NL neurons. The response is apparently mediated by GABA$_A$ receptors and can block the discharges of NL neurons. GABA-induced depolarization has been observed previously in NM and NL neurons (Hyson et al., 1995; Lu et al., 1997; Funabiki et al., 1998). In those studies, GABA was either bath-applied, briefly puffed locally onto a neuron, or synaptically evoked by local extracellular stimulation in the presence of glu-

tamate receptor antagonists. GABA produces long depolarizations up to 20 mV with an associated decrease in input resistance (Hyson et al., 1995; Funabiki et al., 1998), although some of the change in input resistance may be attributable to opening of low-threshold K$^+$ channels caused by depolarization. Synaptically evoked GABAergic responses have been recorded under voltage clamp in NM and NL, showing inward currents lasting up to 60 msec and reversing at E_{Cl} (Lu et al., 1997; Funabiki et al., 1998). The long duration of PSPs evoked by a single shock to the SON is consistent with the duration of spontaneous GABAergic PSPs (Fig. 11) and GABAergic currents recorded in NM and NL (Lu et al., 1997; Funabiki et al., 1998). In addition, the GABAergic responses we recorded in NL were also depolarizing, consistent with our calculated Cl$^-$ equilibrium potential at -34 mV. The present study was the first to demonstrate that such depolarizing GABAergic inhibition of NL neurons could be evoked by direct stimulation of the SON.

SON-evoked inhibition of NL neurons is of importance in modulating coincidence detection in at least two ways; both are associated with elevated membrane conductance in NL neurons. First, elevated membrane conductance during SON activation will reduce the membrane time constant, speeding the rise and decay of excitatory PSPs to allow higher resolution of interaural time delay. Second, when membrane conductance is increased, greater excitatory current is required to reach threshold, which is important in preventing monaural summation at high sound intensity. Because NL neurons receive a large number of NM inputs from both sides of the brainstem, synchrony of firing from either side alone could lead to monaural summation that degrades binaural coincidence detection (Sullivan and Konishi, 1984; Konishi et al., 1988). Because the SON is innervated by the ipsilateral NA that is involved in intensity coding, the firing rate of SON neurons is graded with the ipsilateral sound intensity, thereby providing inhibition at a level reflecting the ipsilateral sound intensity and reducing monaural summation, especially at high sound intensity. According to the present study, the SON is both morphologically and physiologically suited for this task. Neurons have extensive dendritic arborization for the convergence of the excitatory inputs. The EPSPs of SON neurons are long-lasting and readily sum under repetitive stimulation. In addition, we have shown that the firing of SON neurons reflects the strength of current injection or presynaptic stimulation but not the temporal pattern of the inputs. All this evidence is supportive and complementary to a previous idea that the SON is involved in controlling the threshold and gain of coincidence detection by nucleus laminaris neurons (Lachica et al., 1994; Peña et al., 1996).

Physiological evidence for the role of inhibition in the processing of interaural delays has emerged from other animals. Using a brain slice preparation, Grothe and Sanes (1993, 1994) found that in addition to excitatory input, glycinergic inhibition could be evoked in the gerbil medial superior olive (MSO), the analog of the avian NL, by strong shock stimuli to the fiber bundle innervating the MSO from the contralateral side. In the barn owl, Fujita and Konishi (1991) showed that the tuning of interaural delays in the inferior colliculus was degraded by bicuculline, suggesting that the selectivity of interaural delays is first formed in NL but sharpened in the inferior colliculus. Other studies have also suggested the involvement of inhibition in the processing of interaural delays. For instance, at nonoptimal binaural delays, the firing rate of MSO neurons decreases to levels below that evoked by monaural stimulation, and inhibition is implicated in this suppression (Goldberg and Brown, 1969; Yin and Chan, 1990).

However, the suppression of binaural responses at particular interaural delays is also accounted for in systems without inhibition (Colburn et al., 1990; Reyes et al., 1996).

Technical considerations

One concern in interpreting the results presented here is the age of the animals studied. Our *in vitro* analyses were performed using late embryos (18- to 20-d-old) mainly to allow easy visualization of the relatively small SON somata. Additionally, fiber tracts between NL and SON were clearly distinguishable in our slices, probably on account of the lower level of overall myelination at these ages. Although the chick auditory brainstem is still structurally and functionally maturing in the first 2 weeks after hatching, studies show that the fundamental features of the circuitry and intrinsic cell properties are already established by E18. Hearing onset in chickens occurs *in ovo*, at E11 (Saunders et al., 1973), and auditory thresholds are near their adult levels by hatching (Rubel, 1978; Rubel and Parks, 1988). *In vitro* electrophysiology and immunohistochemical studies in NM and NL have found equivalent results between young chickens (ages 1–3 weeks) and late embryos (Smith and Rubel, 1979; Young and Rubel, 1986; Hyson et al., 1995). In addition, our study found no apparent morphological differences between biocytin-filled SON neurons from embryonic brainstem slices and retrogradely labeled SON neurons of 2-week-old hatchlings (data not shown). A previous immunocytochemical study indicates that projections from the SON to NM are present in embryos as early as E12 (Code et al., 1989). Given these observations, the physiological findings reported here should be qualitatively similar to what would be found in mature animals. However, we cannot rule out the possibility that some features observed in the present study, including the long-lasting EPSPs of SON neurons, may undergo some changes in later development.

A second concern is the contradictory findings on the laterality of projections from SON to NM, NA, and NL. In an earlier study, we reported that SON neurons project bilaterally to the cochlear nuclei and NL (Lachica et al., 1994). In that study we used horseradish peroxidase with or without cholera toxin injections into the dorsal brainstem and found a ratio of ~2:1 (ipsilateral: contralateral) projecting SON neurons. In the present study, using lysine-fixable dextrans, the ratio of ipsilateral:contralateral projections was much greater (~20:1). This difference is difficult to understand and requires further experiments. The ages of the subjects were similar (1–2 weeks after hatching). Either the differences in the tracers or "spill over" of the injected materials to the opposite side of the brain appear as possible explanations.

A final issue to consider is the conditions under which we observed the depolarizing responses in NL neurons in response to SON stimulation. Although the NL intracellular $[Cl^-]$ is not known, given the $[Cl^-]$ in our patch pipettes it is not surprising that a depolarizing potential was recorded. However, this response polarity may reflect the natural or undisturbed Cl^- equilibrium for NL neurons. Using intracellular sharp electrodes filled with potassium acetate, Hyson et al. (1995) recorded a similar depolarization of NL neurons in response to application of GABA in chick brainstem slices. It has also been shown that in the mammalian auditory system and other systems, intracellular $[Cl^-]$ declines during development so that GABA and glycine cause depolarization at early developmental stages and hyperpolarization later in development (Kandler and Friauf, 1995; Oh et al., 1995; Tia et al., 1996; Backus et al., 1998; Hollrigel and Soltesz, 1998). Whether or not the same change in Cl^- equilib-

rium occurs in the development of NL neurons is unknown, although the study of Hyson et al. (1995) used chicks between 1 and 2 weeks old, a time when all properties of these regions are thought to be mature, and found similar results to our observations.

REFERENCES

Boord RL (1969) The anatomy of the avian auditory system. Ann NY Acad Sci 167:147–155.

Backus KH, Deitmer JW, Friauf E (1998) Glycine-activated currents are changed by coincident membrane depolarization in developing rat auditory brainstem neurons. J Physiol (Lond) 507:783–794.

Carr CE, Boudreau RE (1991) Central projections of auditory nerve fibers in the barn owl. J Comp Neurol 314:306–318.

Carr CE, Boudreau RE (1993) Organization of the nucleus magnocellularis and the nucleus laminaris in the barn owl: encoding and measuring interaural time differences. J Comp Neurol 334:337–355.

Carr CE, Konishi M (1988) Axonal delay lines for time measurement in the owl's brainstem. Proc Natl Acad Sci USA 85:8311–8315.

Carr CE, Konishi M (1990) A circuit for detection of interaural time differences in the brainstem of the barn owl. J Neurosci 10:3227–3246.

Carr CE, Fujita I, Konishi M (1989) Distribution of GABAergic neurons and terminals in the auditory system of the barn owl. J Comp Neurol 286:190–207.

Code RA, Burd GD, Rubel EW (1989) Development of GABA immunoreactivity in brainstem auditory nuclei of the chick: ontogeny of gradients in terminal staining. J Comp Neurol 284:504–518.

Code RA, Durham D, Rubel EW (1991) Effects of cochlear removal on GABAergic terminals in nucleus magnocellularis of the chicken. J Comp Neurol 301:643–654.

Conlee JW, Parks TN (1986) Origin of ascending projections to the nucleus mesencephalicus lateralis pars dorsalis in the chicken. J Comp Neurol 367:96–113.

Colburn HS, Han Y, Culotta CP (1990) Coincidence model of MSO responses. Hear Res 49:335–346.

Fujita I, Konishi M (1991) The role of GABAergic inhibition in processing of interaural time difference in the owl's auditory system. J Neurosci 11:722–739.

Funabiki K, Koyano K, Ohmori H (1998) The role of GABAergic inputs from coincidence detection in the nucleus laminaris of the chick. J Physiol (Lond) 508: 851–869.

Goldberg JM, Brown PB (1969) Responses of binaural neurons in the dog superior olivary complex to dichotic tonal stimuli: some physiological mechanisms of sound localization. J Neurophysiol 32:613–636.

Grothe B, Sanes DH (1993) Bilateral inhibition by glycinergic afferents in the medial superior olive. J Neurophysiol 69:1192–1196.

Grothe B, Sanes DH (1994) Synaptic inhibition influences the temporal coding properties of medial superior olivary neurons: an *in vitro* study. J Neurosci 14:1701–1709.

Hackett JT, Jackson H, Rubel EW (1982) Synaptic excitation of the second and third order auditory neurons in the avian brain stem. Neuroscience 7:1455–1469.

Hollrigel GS, Soltesz I (1998) Slow kinetics of miniature IPSCs during early postnatal development in granule cells of the dentate gyrus. J Neurosci 17:5119–5128.

Hyson RL, Rubel EW (1989) Transneuronal regulation of protein synthesis in the brain-stem auditory system of the chick requires synaptic activation. J Neurosci 9:2835–2845.

Hyson RL, Sadler KA (1995) Differential distribution of GABA receptor subunits in nucleus magnocellularis and nucleus laminaris of the chick. Assoc Res Otolaryngol [Abstr] 18:33.

Hyson RL, Reyes AD, Rubel EW (1995) A depolarizing inhibitory response to GABA in brainstem auditory neurons of the chick. Brain Res 667:117–126.

Jackson H, Parks TN (1982) Functional synapse elimination in the developing avian cochlear nucleus with simultaneous reduction in cochlear nerve branching. J Neurosci 2:1736–1743.

Jhaveri S, Morest DK (1982a) Neuronal architecture in nucleus magnocellularis of the chicken auditory system with observations on nucleus laminaris: a light and electron microscope study. Neuroscience 7:809–836.

Jhaveri S, Morest DK (1982b) Sequential alterations of neuronal architecture in nucleus magnocellularis of the developing chicken: a Golgi study. Neuroscience 7:837–853.

Joseph AW, Hyson RL (1993) Coincidence detection by binaural neurons in the chick brain stem. J Neurophysiol 69:1197–1211.

Kandler K, Friauf E (1995) Development of glycinergic and glutamatergic synaptic transmission in the auditory brainstem of perinatal rats. J Neurosci 15:6890–6904.

Konishi M, Takahashi TT, Wagner H, Sullivan WE, Carr CE (1988) Neurophysiological and anatomical substrates of sound localization in the owl. In: Auditory function (Edelman GM, Gall WE, Cowan WM, eds), pp 721–745. New York: Wiley.

Köppl C (1994) Auditory nerve terminals in the cochlear nucleus magnocellularis: differences between low and high frequency. J Comp Neurol 339:438–446.

Lachica EA, Rübsamen R, and Rubel EW (1994) GABAergic terminals in nucleus magnocellularis and nucleus laminaris originate from the superior olivary nucleus. J Comp Neurol 348:403–418.

Lu T, Oertel D, Trussell L (1997) GABA-evoked conductance in the avian cochlear nucleus. Annual Neuroscience Conference [Abstr] 605.5.

Müller CM (1987) r-aminobutyric acid immunoreactivity in brainstem auditory nuclei of the chicken. Neurosci lett 77:272–276.

Oh K, Lee C, Gibbs JW, Coulter DA (1995) Postnatal development of GABA$_A$ receptor function in somatosensory thalamus and cortex: whole-cell voltage-clamp recordings in acutely isolated rat neurons. J Neurosci 15:1341–1351.

Overholt EM, Rubel EW, Hyson RL (1992) A circuit for coding interaural time differences in the chick brain stem. J Neurosci 12(5):1698–1708.

Parks TN (1981) Morphology of axosomatic endings in an avian cochlear nucleus: nucleus magnocellularis of the chicken. J Comp Neurol 203:425–440.

Parks TN, Rubel EW (1975) Organization and development of the brain stem auditory nuclei of the chicken: organization of projections from nucleus magnocellularis to nucleus laminaris. J Comp Neurol 164:435–448.

Parks TN, Rubel EW (1978) Organization and development of the brain stem auditory nuclei of the chicken. J Comp Neurol 180:439–448.

Peña JL, Viete S, Albech Y, Konishi M (1996) Tolerance to intense sound of binaural coincidence detection in the owl's nucleus laminaris. J Neurosci 16:7046–7054.

Rall W (1969) Time constants and electrotonic length of membrane cylinders and neurons. Biophys J 9:1483–1508.

Raman IM, Trussell L O (1992) The kinetics of the response to glutamate and kainate in neurons of the avian cochlear nucleus. Neuron 9:173–186.

Raman IM, Zhang S, Trussell JO (1994) Pathway-specific variants of AMPA receptors and their contribution to neuronal signaling. J Neurosci 14:4998–5010.

Ramón y Cajal S (1971) The acoustic nerve: its cochlear branch or cochlear nerve (translated from Histologie du Systèmè Nerveux de l'Homme et des Vertèbrès, Tome I, pp 774–838:1952). National Technical Information Service Publication No. PB-205 473.

Reyes AD, Rubel EW, Spain WJ (1994) Membrane properties underlying the firing of neurons in the avian cochlear nucleus. J Neurosci 14:5352–5364.

Reyes AD, Rubel EW, Spain WJ (1996) *In vitro* analysis of optimal stimuli for phase-locking and time-delayed modulation of firing in avian nucleus laminaris neurons. J Neurosci 16:993–1007.

Rubel EW (1978) Ontogeny of structure and function in the vertebrate auditory system. In: Handbook of sensory physiology, Vol 9, (Jacobson M, ed) pp 135–237. New York: Springer.

Rubel EW, Parks TN (1975) Organization and development of brain stem auditory nuclei of the chicken: tonotopic organization of n. magnocellularis and n. laminaris. J Comp Neurol 164:411–434.

Rubel EW, Parks TN (1988) Organization and development of the avian brainstem auditory system. In: Auditory function (Edelman GM, Gall WE, Cowan WM, eds), pp 3–92. New York: Wiley.

Saunders JC, Cole RB, Gates GR (1973) The development of auditory evoked responses in the cochlea and cochlear nuclei of the chick. Brain Res 63:59–74.

Smith DJ, Rubel EW (1979) Organization and development of brain stem auditory nuclei of the chicken: dendritic gradients in nucleus laminaris. J Comp Neurol 186:213–240.

Sullivan WE, Konishi M (1984) Segregation of stimulus phase and intensity coding in the cochlear nucleus of the barn owl. J Neurosci 4:1787–1799.

Takahashi T, Konishi M (1988) The projections of nucleus angularis and nucleus laminaris to the lateral lemnisical nuclear complex of the barn owl. J Comp Neurol 274:212–238.

Tia S, Wang JF, Kotchabhakdi N, Vicini S (1996) Developmental changes of inhibitory synaptic currents in cerebellar granule neurons: role of GABA$_A$ receptor α6 subunit. J Neurosci 16:3630–3640.

Trussell LO, Zhang S, Raman IM (1993) Desensitization of AMPA receptors upon multi-quantal neurotransmitter release. Neuron 10:1185–1196.

von Bartheld CS, Code RA, Rubel EW (1989) GABAergic neurons in brainstem auditory nuclei of the chick: distribution, morphology and connectivity. J Comp Neurol 287:470–483.

Warchol ME, Dallos P (1990) Neural coding in the chick cochlear nucleus. J Comp Physiol 166:721–734.

Yin TCT, Chan JCK (1990) Interaural time sensitivity in medial superior olive of cat. J Neurophysiol 64:465–488.

Young SR, Rubel EW (1983) Frequency specific projections of individual neurons in chick brain stem auditory nuclei. J Neurosci 7:1373–1378.

Young SR, Rubel EW (1986) Embryogenesis of arborization pattern and topography of individual axons in n. laminaris of the chick brain stem. J Comp Neurol 254:425–459.

Zhang S, Trussell LO (1994) Voltage clamp analysis of excitatory synaptic transmission in the avian nucleus magnocellularis. J Physiol (Lond) 480:123–136.